Chapter 8

Applications of Nanodot Arrays in

Field Emission Triodes

8.1 Introduction

Cold-cathode field emitter arrays (FEAs) have been the subject of intense research, primarily because of the potential applications of the technology, such as field emission flat panel displays[Itoh 2002-514; 2004-1362], cold-cathode microwave devices[Han 2004-1636], and electron guns in X-ray tubes[Yue 2002-355]. For the practical applications, FEAs must have a low turn-on voltage, high emission current density, high current stability, and long lifetime. In the past decade, numerous nanostructured materials, including carbon nanotubes (CNTs)[Heer 1995-1179; Saito 2000-169; Bonard 1998-918], carbon nanoparticles (CNPs)[Park 2002-358; 2003-562], IrO_2 nanorods[Chen 2004-1552], ZnO nanowires[Tseng 2003-811; Jo 2003-4821], MoS_2 nanoflowers[Li 2003-1962], etc., have been extensively studied to achieve the goal. The low-dimensional nanostructures with small radii of curvature give strong field enhancement and thus increase emission current, making them highly promising for electron field emitter applications. However, it is still a challenge to fabricate the uniform nanostructures over a large area with an inexpensive procedure. In Chapter 7, we employed nanoporous anodic aluminum oxide (AAO) films as the mask for local anodic oxidation of metal films to fabricate nanodot arrays of metal oxides. By using the AAO templates as the anodization mask for metallic thin films, one can realize ordered arrays of oxide nanodots with a very high packing density (as high as 10^{10} cm^{-2}) and narrow size distribution. The attractiveness of applying this technique in FEAs production mainly relies on its low processing cost and excellent uniformity over a large area compared with chemical vapor deposition (CVD) process which is widely introduced to synthesize the nanostructured materials. In addition, the obtained nanodots consisted of metal oxides provide stable chemical and structural properties, whereas metallic FEAs (e.g., molybdenum and niobium tips) have shown increased tendency for oxidation during the operation, leading to the emission current fluctuation[Itoh 1993-647; Chalamala 1999-303]. Tatarenko *et al.*[Tatarenko 1999-647] have demonstrated

that such oxide nanodots with a high geometrical enhancement promise to be very fruitful in field emission. However, field emission controlled by an integrated active device or extraction gate electrode is essential for low driving voltage, full gray scales, and high-resolution field emission displays (FEDs)[Hirano 1996-L861; Cheng 2001-H5]. From this point of view, a triode-type field emission device using the self-organized nanodots as FEAs was proposed and fabricated in this study. The fabrication process is an easily controllable and integrated circuit (IC) technology compatible process, which shows potential for application in field emission displays and vacuum microelectronics.

8.2 Field emission from nanodot arrays

Figure 8-1 depicts the schemata of the overall process for the fabrication of the nanodot-based field emission triodes, in which Figures 8-1(a)-(c) are the steps for the preparation of the nanodot emitters. At first, a 200-nm-thick titanium film and a 3-μm-thick aluminum film were sequentially deposited on a *p*-silicon (100) substrate by thermal evaporation in a high vacuum chamber ($< 5\times10^{-7}$ Torr). Then, the as-deposited Al/Ti bilayered films were directly oxidized by electrochemical anodization, which was
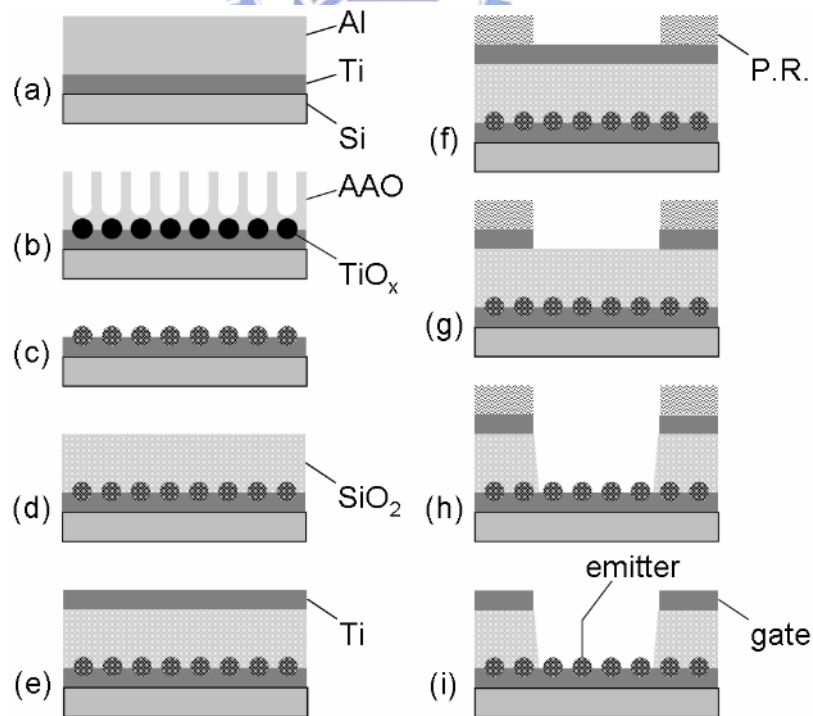
Figure 8-1 Fabrication procedures of the nanodot-based field emission triodes: (a) Titanium and aluminum deposition, (b) anodization, (c) AAO removal and vacuum annealing, (d) TEOS oxide deposition, (e) titanium deposition, (f) pattern formation, (g) titanium dry etching, (h) TEOS oxide dry etching, and (i) photoresist lift-off.
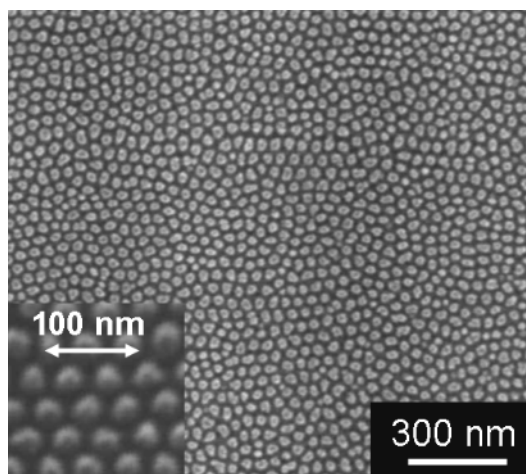
Figure 8-2 Top-view FE-SEM image of the titanium oxide nanodot arrays after the nanoporous AAO template was removed by a mixed solution of phosphoric acid and chromic acid. The inset is the side-view image of the nanodots.

performed in a 0.6 M sulfuric acid (H_2SO_4) solution at 21 ^oC under a constant polarization voltage of 20 V. The anodization is regarded to involve two oxidation stages, i.e., anodic oxidations of the aluminum layer and the underlying titanium layer, as described detailed in Chapter 7. During the first stage, the upper aluminum layer was oxidized to form nanoporous AAO, which was then used as a mask for local anodization of the underlying titanium layer. While the downward grown AAO pore channels approached the Al/Ti interface, anodic oxidation of the titanium layer was initiated. Because the titanium oxidation was confined in the nanometer-sized pore area of the initially formed AAO, dome-shaped titanium oxide nanodots were formed between the remaining titanium layer and the top AAO film. Figure 8-2 shows the top-view field-emission scanning electron microscopy (FE-SEM) (Hitachi S-4000) image of the titanium oxide nanodot arrays after removing the nanoporous AAO film. The self-organized nanodots have an average diameter of about 40 nm and an average height of about 30 nm. The close-packed nanodots duplicating the pattern of AAO nanopores are uniform in arrangement and shape over the whole sample (2-inch square) with a dot number density as high as 4×10^{10} dots/cm^2. The diameter of the nanodots is tunable in the range of ten to hundred nanometers, which is dependent upon anodization parameters.

Figure 8-3(a) shows Auger electron spectroscopy (AES) (VG Microlab 310F) depth profiles for an as-prepared titanium oxide nanodot presenting changes in percentage of titanium, aluminum, oxygen, and silicon atoms with the time of argon ion sputtering. It is obvious that the nanodot is mainly composed of titanium and oxygen.
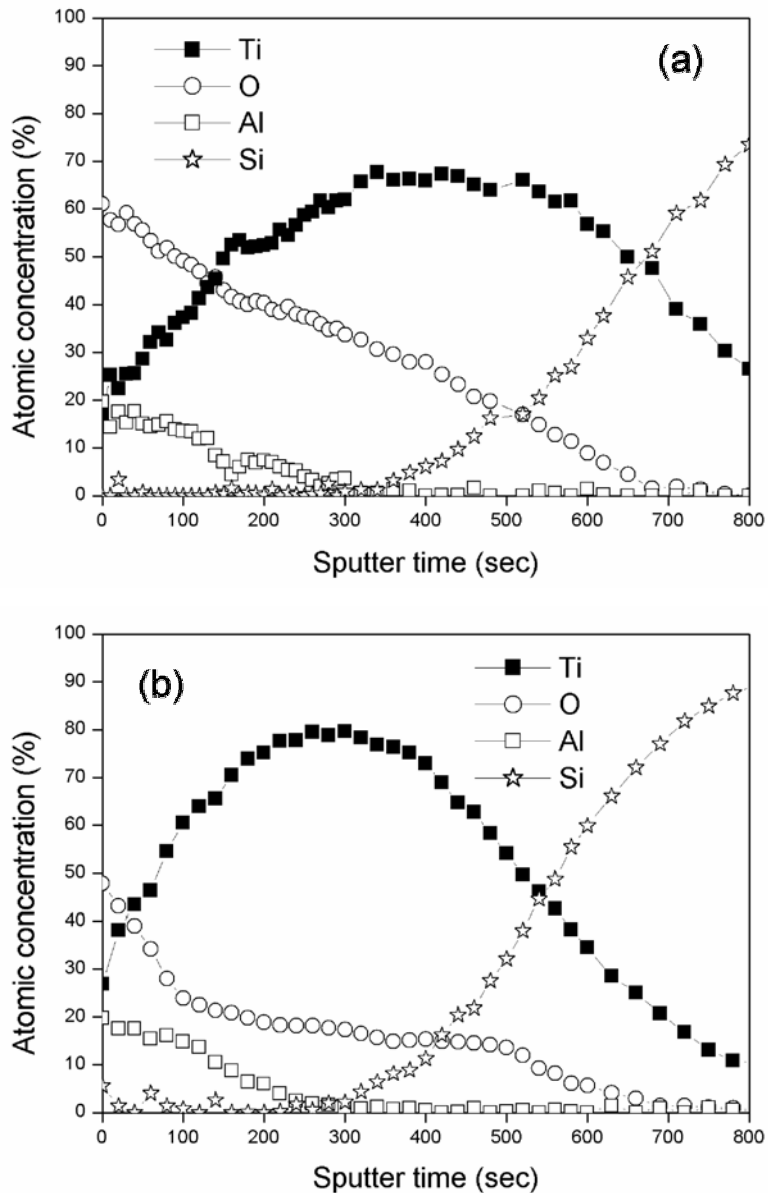
Figure 8-3 Auger electron profiles of (a) an as-prepared and (b) an annealed titanium oxide nanodot presenting changes in percentage of titanium, aluminum, oxygen, and silicon atoms with the time of argon ion sputtering.

Moreover, aluminum signals were also detected, which probably correlates with the aluminum remaining between the dots. As shown in Figure 7-11, there are un-anodized aluminum residues surrounding the nanodots. While the ion sputtering begin, the titanium atom concentration increases and oxygen atom concentration decreases gradually. During the initial 140 sec of the sputtering, the oxygen concentration is significantly higher than the titanium implying that there are oxygen rich titanium oxides at the nanodot tops. These titanium oxides would work as a resistor reducing conductivity of the current path to the emission site, owing to their high resistance
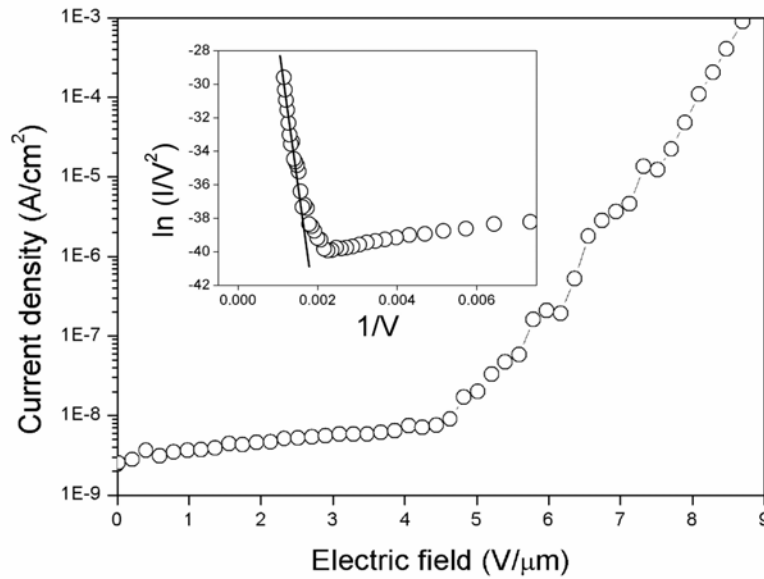
Figure 8-4 Field emission current density as a function of electric field for the self-organized titanium oxide nanodot arrays after the vacuum annealing. The inset shows the corresponding Fowler-Nordheim plot.

nature. For a titanium dioxide film prepared by solid-state reactions, the electrical resistivity of the film can be more than 10^{10} Ω-cm[Yokota 1998-109]. In order to function as a field emitter, it is necessary to reduce the electrical resistance of the titanium oxide nanodots by means of vacuum annealing treatment. Annealing was performed at 450 ^{o}C in a high vacuum furnace (about 1×10^{-7} Torr) for 2 hour. The vacuum annealing would promote the diffusion of oxygen from the nanodot body to the underlying titanium film. Figure 8-3(b) shows AES depth profiles for a nanodot after the annealing. Almost immediately after the beginning of the ion sputtering, the oxygen content decreases sharply from 50 to 20% and then decreases slowly to less than 15%. The annealing treatment leads to decrease the oxygen concentration in the nanodot body and on the nanodot surface as well. Consequently, the metallic phase in the nanodot became dominant and oxygen was uniformly distributed over the nanodots, making it more applicable for field emission.

Figure 8-4 shows the field emission current density (J) as a function of applied electric field (E) for the titanium oxide nanodot arrays after the vacuum annealing. Measurements were conducted by the simple diode configuration and performed in a high vacuum chamber (about 10^{-6} Torr) at room temperature. The distance between the nanodots and anode was about 100 μm. The annealed nanodots show a turn-on field (E_{to}) at 7.2 V/μm, in which E_{to} is here defined as the electric field required for the emission

current density of 10 μA/cm^2 for typical operation in FEDs[Bonard 1998-918]. The emission current density reached 1 mA/cm^2 at an applied electric field of about 8.7 V/μm. The inset in Figure 8-4 shows the corresponding Fowler-Nordheim (F-N) plot of the field emission data. After passing the turning point, the F-N plot exhibits a reasonably linear relationship, suggesting a field electron emission mechanism in accordance with the F-N model. The slope of the F-N plot is equal to $-Bd\varphi^{3/2}/\beta$, where $B = 6.83\times10^9$ (V eV$^{-3/2}$ m^{-1}), d is the distance between emitter tip and anode, φ is the work function of emitter, and β is the field enhancement factor. From the equation above, the β value was estimated to be about 1936 by assuming a nanodot work function of 7.3 eV (work function of TiO$_2$). The estimated β value is comparable with the high field enhanced material such as multi-walled CNTs (β = 1500 to 4500)[Yoon 2004-825], demonstrating that the nanosized dots are promising emitting material for applications in FEDs. Using a simple concentric sphere model[Brodie 1994-1006], the field enhancement factor can be approximated as

$$\beta = \frac{d^2}{\xi R_t(d - R_t)} \approx \frac{d}{\xi R_t}, \text{ for } R_t \ll d \qquad (8.1)$$

where R_t is the emitter-tip radius and ξ accounts for the effect of the emitter shank with a value between 1 and 5. Under the field emission measurement condition, in which the separation between the anode and the nanodots was 100 μm, the ξ value of the nanodots of about 40 nm in diameter was estimated to be about 2.5. The small ξ value suggests that the dome structure of nanodots fabricated by AAO templation can result in a large field emission enhancement.

8.3 Fabrication and characterization of field emission triodes

After the nanodot emitter production, the succeeding fabrication procedures for the triode devices are shown schematically in Figures 8-1(d)-(i). As shown in Figure 8-1(d), a 1.5-μm-thick dielectric layer of tetraethoxysilane (TEOS) oxide was directly deposited onto the nanodot coated substrates using a plasma-enhanced CVD (PECVD) system. A 600-nm-thick titanium layer was then deposited as the gate electrode by thermal evaporation [Figure 8-1(e)]. By photolithography, a gate aperture array of 20 μm diameter was defined. Reactive ion etching (RIE) was performed using a Cl$_2$/BCl$_3$
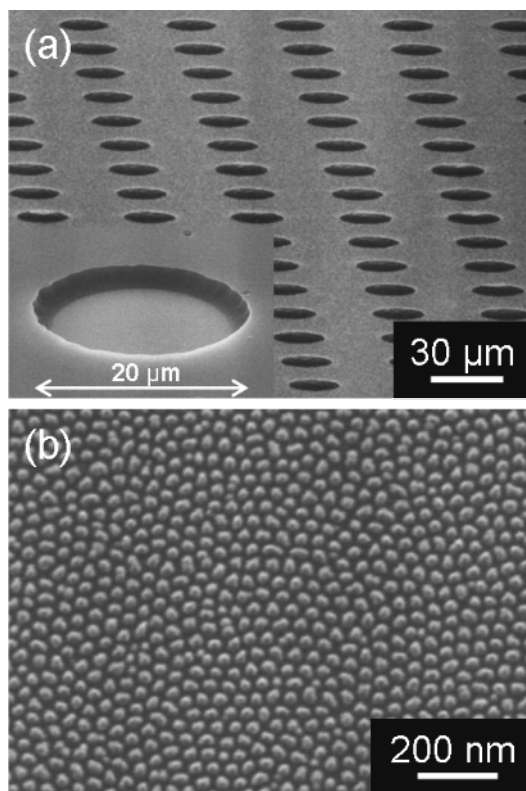
Figure 8-5 (a) Side-view FE-SEM image of the nanodot-based field emission triode array. The inset shows a higher magnification image. (b) Side-view FE-SEM image of the nanodot emitter arrays inside the gate aperture.

plasma to transfer the aperture pattern into the titanium layer [Figure 8-1(g)], followed by RIE of the TEOS oxide layer using a CF_4/CHF_3 plasma to release the buried nanodot arrays [Figure 8-1(h)], carried out in a high density plasma RIE (HDP-RIE) system. The working pressure of the HDP-RIE system was 1×10^{-2} Torr with an inductively coupled plasma (ICP) power of 750 W and a rf bias power of 120 W. After RIE the structures were dipped into a dilute hydrogen fluoride (DHF) solution for a few seconds to sweep away the residual TEOS oxide on the nanodot surface. Finally, the photoresist was removed by acetone [Figure 8-1(i)] and the nanodot triodes were completed. A side-view FE-SEM image of the finished device arrays is shown in Figure 8-5(a). The fabricated device contains 16×16 arrays of gated cathode cells. Figure 8-5(b) shows a higher magnification image of the nanodot emitter arrays inside the gate aperture. The FE-SEM image reveals that the nanodots could survive the DHF dip and the RIE process in a CF_4/CHF_3 plasma for TEOS oxide removal and maintain their geometrical configuration without discernable damage. This allowed us to fabricate the nanodot-based devices using standard microfabrication techniques and provided feasibilities of process variation.
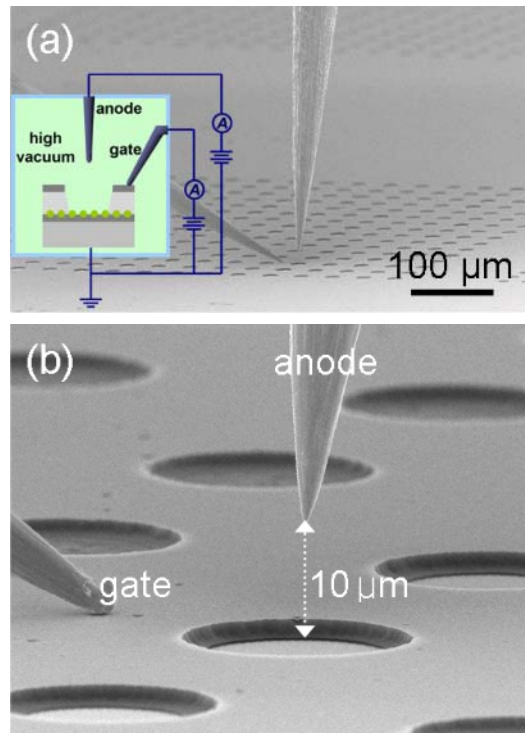
Figure 8-6 Side-view TF-SEM image of the moveable tungsten microprobes and the field emission triode array showing the configuration for the field emission measurements. (a) Low magnification and (b) high magnification images.

The field emission properties of the triode devices were characterized by moveable tungsten microprobes set up inside a thermal field-emission SEM (TF-SEM) (JEOL JSM-6500F) system with a base pressure of 10^{-7} Torr. The microprobes with a minimum step size of 10 nm in the *x-y-z* directions were controlled by piezo driven linear nanomotors. Figures 8-6(a) and (b) show *in situ* SEM images displaying the configuration for the field emission measurements. The cathode (emitter) was grounded and the gate electrode was connected to a microprobe applied with a voltage swept positively from 0 to 120 V to extract electrons from cathode. The field emitted electrons were collected by placing a microprobe (anode) about 10 μm away from the gate aperture. A constant positive voltage of 50 V was applied to the anode probe. High voltage source-measure units (Keithley 237) were connected to each microprobe to apply the dc voltage and measure the field emitted current.

Figure 8-7 shows the gate-voltage dependence of emission currents of the nanodot triodes. The electron emission started at a gate voltage of about 45 V, and the anode current reached a level of 80 nA when the gate voltage was increased to 120 V. The measured anode current was mainly provided by one individual cathode cell (gate aperture) under the anode probe, and thus the anode current of 80 nA measured at a gate
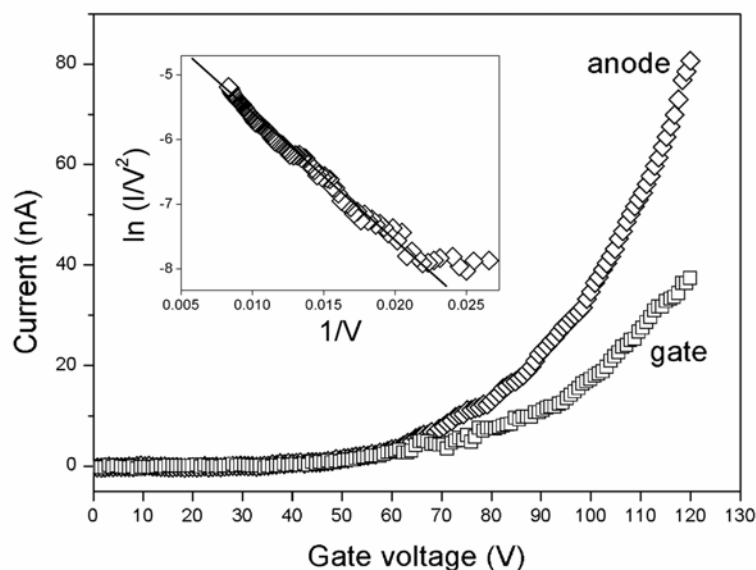
Figure 8-7 Gate-voltage dependence of anode and gate current. The inset shows the corresponding Fowler-Nordheim plot of the anode current.

voltage of 120 V corresponds to a considerably high emission current density of 25 mA/cm^2 (one aperture area about 3×10^{-6} cm^2). Because the electric field produced by the anode probe is negligibly weak for the neighboring cathode cells (electric field is nearly 1 order of magnitude lower)[Baylor 2002-4602], the measured anode current can be regarded as the field emitted current derived from one cathode cell under the anode probe. This allowed us to measure the field emission properties of individual gated cathode cells by the microprobes. We have compared the emission results of the cathode cells with one the others and only little difference between them was observed, which was essentially contributed to the excellent uniformity of the nanodot emitters. The F-N plot of the anode current, shown in the inset in Figure 8-7, also exhibit a linear fit confirming that the field emitted electrons due to gate bias was responsible for this current. However, the measured leakage current to the gate electrode is about 50% of the current reaching the anode probe as shown in Figure 8-7. The detection of the significantly high gate current is owing to that the whole 16×16 arrays of gated cathode cells are controlled by the same gate electrode, and therefore leakage current of whole cathode cells was measured simultaneously. In contrast, the anode current was practically measured from only one cathode cell.

8.4 Summary

The nanodot-based field emission triode has been successfully fabricated and

characterized its field emission properties. The emitter arrays of titanium oxide nanodot were prepared from Al/Ti bilayered films on silicon wafers by electrochemical anodization. Field emission properties of individual gated cathode cells investigated by moveable microprobes imply a low gate turn-on voltage of 45 V and considerably high emission current density of 25 mA/cm^2 at 120 V. The excellent electric properties and easily controllable fabrication process of the nanodot triodes show potential for application in field emission displays and vacuum microelectronics.